Comparison of Potential and Activation Based Formulations for the Inverse Problem of Electrocardiology

Leo K. Cheng, John M. Bodley and Andrew J. Pullan

Abstract

Two predominant source formulations for the inverse problem of electrocardiology currently exist. They involve the reconstruction of epicardial potentials or myocardial activation times from non-invasively recorded torso surface potentials. Each of these formulations have their advantages, however, they have not been systematically compared against each other. We present results from a simulation study which compared a number of epicardial potential (Tikhonov, Truncated SVD, Greensite-Tikhonov and Greensite-TSVD) and a myocardial activation time formulation for the inverse problem of electrocardiology. A number of different methods were also used to determine the appropriate level of regularization (optimal, L-curve, zero-crossing, CRESO) to apply to each formulation.

The simulation study was conducted using an anatomically based boundary element porcine model with a variety of cardiac sources. Varying levels of geometric error were introduced to the system and solutions were computed using each of the inverse algorithms. Results show that under pure Gaussian noise potential based methods performed best at low noise levels while the activation based method was less effected by higher noise levels. In the presence of correlated geometric error the activation based method out performed the potential methods, with the Greensite-Tikhonov method being the most favored potential based method when using the L-curve or zero-crossing method to determine the regularization parameter.

Keywords

epicardial potential inverse, myocardial activation inverse, simulation study, comparison.

L K Cheng, J M Bodley and A J Pullan are with the Bioengineering Institute, The University of Auckland, Private Bag 92019, New Zealand. (e-mail: {l.cheng|a.pullan}@auckland.ac.nz).

I. INTRODUCTION

Reconstruction of cardiac electrophysiological activity from remotely measured thoracic ECG recordings is known as the inverse problem of electrocardiography [1], [2]. Potential recordings obtained on the torso surface provide a spatially filtered, low resolution representation of the electrical events which occur within the myocardium.

Unless measurements are made directly on the active muscle, reconstruction of the heart activity at the cellular level is impossible [3]. This is because it is possible to generate the same remote electrical recordings from different configurations of cells. This fact lead to early attempts at solving the inverse problem being restricted to a small number of fixed or moving dipoles. At the body surface it has been shown that the number of independent recordings that can be obtained under a variety of conditions is of the order of $20 - 40$ although the sites at which these appear may vary [4], [5]. It follows then that the number of independent parameters or features that one can detect is also relatively low (providing one explanation why it becomes increasingly difficult to obtain anything meaningful from multiple dipole source inverse formulations when the number of dipoles increases). The reconstruction of dipole configurations also provides little in sight into the actual electrical activity which is occurring within the heart.

The first relationship between epicardial and body surface potentials was first suggested by Zablow [6] and his ideas were later extended further using simple geometry by Martin [7]. This integral relationship between epicardial and body surface potentials, opened up a new approach to the inverse problem, namely that of reconstructing the epicardial surface potentials. By defining the problem in terms of epicardial potentials the problem is now uniquely determined [3], [7] (unlike the equivalent dipole formulation). The epicardial potentials have also been shown to closely reflect the electrical activity which is occurring within the myocardium [9].

Another approach has involved the reconstruction of the myocardial activation sequence itself [10]. The reconstruction of the activation wavefront provides a closer representation of the true underlying events that are occurring. Unlike a multiple dipole formulation, both the epicardial potential and activation based formulations are unique, although inherently ill-posed in the sense of Hadamard: the solution does not depend continuously on the data and small errors in the input can results in large disproportionate errors in the computed solution [11]. Various attempts have been employed to overcome this difficulty, giving rise to many of the different inverse formulations currently in existence [12], [13], [14]. The large variety of inverse algorithms, each being validated using different methods and measures, has lead to uncertainties in a preferred direction to take for improving existing algorithms.

Previous studies investigating the effectiveness of the inverse algorithms have usually concentrated on a single method. Various Tikhonov regularization schemes have been extensively investigated using both concentric sphere models and realistic geometric models [15], [16]. The potential based method presented in [17] which is both temporally and spatially regularized (hereafter called the Greensite method) presented results using a simulated cardiac

source [17] and a realistic torso geometry. An activation inverse algorithm based on the Critical Point Theorem [18] was tested by using both simulated and experimental data with realistic torso geometry [19]. These independent studies using different geometries and cardiac sources have lead to difficulties in comparing the relative performances of each of these algorithms and formulations.

We aim to carefully analyze and compare the performance of a variety of inverse schemes (both activation and potentials based) using an anatomically based porcine model with a range of cardiac source models. By doing this, we aim to gain a better understanding not only of the limits of each different approach, but also of the relative strengths and merits of each respective technique.

It should be pointed out that all the techniques used in this work are non-linear with respect to each cardiac source. This means that the results for difference sources are not additive and that trends observed with one cardiac electrophysiological state may not be the same as those observed with another state. However, it is hoped that the simulation results presented here will at least be a useful guide.

A brief review of a number of common epicardial inverse procedures is given, followed by a description of an activation based inverse approach. The geometric domain on which the tests are carried out is then described, together with the different cardiac sources used in this study. Initial results showing the relative performances between the different inverse algorithms under both Gaussian noise and in the presence of known amounts of geometrical error are presented.

II. Reconstruction of Myocardial Activation Times and Epicardial Potentials

The reconstruction of epicardial potentials or myocardial activation times are the two main solutions for the inverse problem of electrocardiology. Each of the inverse algorithms used throughout the simulations have been previously described. However, we provide a brief description of each of these algorithms in the following sections for completeness and to maintain consistency of notation.

A. Potential Based Inverse Algorithms

By posing the inverse problem in terms of reconstructing epicardial potentials, the solution is unique, however, because the inverse problem is ill-posed the formulation is also inherently unstable. The major difficulty with such discrete ill-posed problems is that the computed solution is sensitive to perturbations. Low levels of signal noise or small geometric error can result in an unbounded solution. Hence it is necessary to incorporate further information about the solution in order to stabilize the problem to obtain a feasible and stable solution.

Currently, two points of view exist to how best to handle the epicardial inverse problem: regularization or imposing additional constraints. The term regularization was first introduced for a certain technique, but now it is accepted to

classify any method to compute a smooth solution as a regularization method [12]. It is necessary to compute a smooth solution which has useful properties in common with the exact solution to the underlying unperturbed problem, by filtering out the high-frequency components associated with small singular values [20]. The basic problem with such a technique is that it is not normally known *a priori* the amount of regularization which is required in order to produce a smooth solution. The second approach to solving the epicardial potential inverse problem is that of imposing *a priori* constraints on the solution. These constraints can relate to physiology or known information about the solution that can be both implicitly present in the formulation of the problem or explicitly defined in the definition.

The standard solution approach to solving the epicardial inverse problem of electrocardiography is based on solving a time series of quasi-static problems given in the form

$$\phi_B(\boldsymbol{x}, t) = \boldsymbol{A}\phi_H(\boldsymbol{y}, t) \tag{1}$$

where $\boldsymbol{A}$ is the geometric noise-corrupted transfer matrix and $\phi_B(\boldsymbol{x}, t)$ is a noise-corrupted body surface potential distribution at location x and $\phi_H(\boldsymbol{y}, t)$ is the unknown heart solution at location y defined at time t. An adequate inverse of the linear operator $\boldsymbol{A}$ is necessary in order to obtain a useful solution $\phi_B(\boldsymbol{x}, t)$. Alternatively we can consider a system of linear equations given by

$$\boldsymbol{\Phi}_B = \boldsymbol{A}\boldsymbol{\Phi}_H \tag{2}$$

where $\boldsymbol{A}$ and $\boldsymbol{\Phi}_B$ are both noise-corrupted linear operators of the solution $\boldsymbol{\Phi}_H$ [21]. The matrices $\boldsymbol{\Phi}_B$ and $\boldsymbol{\Phi}_H$ have columns which are spatial vectors of potentials at a discrete locations on the heart and torso surface while each row is a time series of potential at a given spatial positions. By solving each column of $\phi_B(\boldsymbol{x}, t)$ to obtain the regularized solution $\phi_H(\boldsymbol{y}, t)$ to (2) we get

$$\phi_H(\boldsymbol{y}, t) = \boldsymbol{A}^{\dagger}_{\lambda_t}[\phi_B(\boldsymbol{x}, t)] \tag{3}$$

where $\boldsymbol{A}^{\dagger}_{\lambda_t}$ is the regularized inverse at time t. The regularized inverse can either represent a Tikhonov regularized inverse with regularization parameter λ_t or a truncated singular value decomposition (TSVD) of $\boldsymbol{A}$ given by the truncation rank λ_t. In practice these two families of regularization methods are the most widely used.

A.1 Tikhonov Regularization

The Tikhonov solution is obtained by minimizing the objective function

$$\phi_H(\boldsymbol{y}, t) = \min \|\boldsymbol{A}\phi_H(\boldsymbol{y}, t) - \phi_B(\boldsymbol{x}, t)\|_2^2 + \lambda_t^2 \|\boldsymbol{R}\phi_H(\boldsymbol{y}, t)\|_2^2 \tag{4}$$

where $\boldsymbol{R}$ is a $N \times N$ constraint matrix and $\|\cdot\|_2$ is the Euclidean norm.

There are three common Tikhonov regularization methods – zero, first and second order. Zero-order Tikhonov has $\boldsymbol{R} = \boldsymbol{I}$, the identity matrix, first-order Tikhonov uses $\boldsymbol{R} = \boldsymbol{G}$ a discrete approximation to the surface gradient operator and the second-order Tikhonov method uses $\boldsymbol{R} = \boldsymbol{L}$ a discrete approximation to the surface Laplacian operator to regularize the system.

The first term in (4) represents the least-squares solution to (2) while the second term constrains the amplitude of the solution for zero-order Tikhonov, the surface gradient for first-order or the surface curvature for second-order Tikhonov in the spatial domain [13]. The constant λ_t is the *regularization parameter* at time t which controls the weight given to the residual and solution norm and controls the degree of smoothing [13].

The inverse for (3) is given by

$$\boldsymbol{A}^{\dagger}_{\lambda_t} = (\boldsymbol{A}^T\boldsymbol{A} + \lambda_t^2\boldsymbol{R}^T\boldsymbol{R})^{-1}\boldsymbol{A}^T \tag{5}$$

The variations of Tikhonov regularization have previously been studied and compared using analytic solutions and a spherical model [22]. It was found that zero-order Tikhonov regularization performed as well as those of higher order, therefore we focus our remaining effort on the zero-order Tikhonov inverse. Substituting (5) into (3) the solution for zero-order Tikhonov gives

$$\begin{aligned}\phi_H(\boldsymbol{y},t) &= (\boldsymbol{A}^T\boldsymbol{A} + \lambda_t^2\boldsymbol{I})^{-1}\boldsymbol{A}^T[\phi_B(\boldsymbol{x},t)] \\ &= \sum_{n=1}^{N} f_n(t)\frac{\langle u_{A,n}(\boldsymbol{x}), \phi_B(\boldsymbol{x},t)\rangle}{\sigma_{A,n}} v_{A,n}(y)\end{aligned} \tag{6}$$

where u and v are the vectors from an SVD decomposition, σ are their corresponding singular values, $\langle\cdot,\cdot\rangle$ denotes the inner dot product of the columns vectors and $f_n(t)$ are the Tikhonov filter factors given by

$$f_n(t) = \frac{\sigma_{A,n}^2}{\sigma_{A,n}^2 + \lambda_t^2} \backsimeq \begin{cases} 1 & \sigma_{A,n} \gg \lambda_t \\ \sigma_{A,n}/\lambda_t^2 & \sigma_{A,n} \ll \lambda_t \end{cases} \tag{7}$$

Hence, the filter factors filter out the contribution of $\phi_H(\boldsymbol{y},t)$ corresponding to the small singular values whilst leaving the singular value decomposition (SVD) components corresponding to large singular values almost unaffected.

A.2 Truncated SVD

Another method of treating the ill-conditioned nature of the transfer matrix $\boldsymbol{A}$ is to derive a new problem with a well-conditioned *rank deficient* transfer matrix [23]. The closest rank-λ_t approximation $\boldsymbol{A}_{\lambda_t}$ to $\boldsymbol{A}$ is easily obtained by truncating an SVD expansion of $\boldsymbol{A}$, *i.e.,*

$$\boldsymbol{A}_{\lambda_t}(\boldsymbol{x},\boldsymbol{y}) = \sum_{n=1}^{\lambda_t} \sigma_{A,n} u_{A,n}(\boldsymbol{x}) v_{A,n}(\boldsymbol{y}) \qquad \lambda_t \leq N \tag{8}$$

The Truncated SVD (TSVD) solution is obtained by minimizing the objective function

$$\phi_H(\boldsymbol{y},t) = \min \|\boldsymbol{A}_{\lambda_t}\phi_H(\boldsymbol{y},t) - \phi_B(\boldsymbol{x},t)\| \tag{9}$$

The inverse for this problem is given by

$$\boldsymbol{A}^{\dagger}_{\lambda_t} = \tilde{\boldsymbol{V}}_A \tilde{\boldsymbol{\Sigma}}_A^{-1} \tilde{\boldsymbol{U}}_A^T \tag{10}$$

where $\tilde{\boldsymbol{U}}_A$ and $\tilde{\boldsymbol{V}}_A$ contain the first λ_t columns of $\boldsymbol{U}_A$ and $\boldsymbol{V}_A$ respectively and $\tilde{\boldsymbol{\Sigma}}_A$ is a $\lambda_t \times \lambda_t$ diagonal sub-matrix of $\boldsymbol{\Sigma}$ (where $\boldsymbol{V_A}$ and $\boldsymbol{U_A}$ are the orthogonal matrices from the SVD of $\boldsymbol{A}$ and $\boldsymbol{\Sigma}$ are corresponding singular values). Substituting (10) into (3), the TSVD solution yields

$$\begin{aligned}\phi_H(\boldsymbol{y},t) &= \tilde{\boldsymbol{V}}_A \tilde{\boldsymbol{\Sigma}}_A^{-1} \tilde{\boldsymbol{U}}_A^T [\phi_B(\boldsymbol{x},t)] \\ &= \sum_{n=1}^{\lambda_t} \frac{\langle u_{A,n}(\boldsymbol{x}), \phi_B(\boldsymbol{x},t)\rangle}{\sigma_{A,n}} v_{A,n}(\boldsymbol{y})\end{aligned} \tag{11}$$

where $\phi_H(\boldsymbol{y},t)$ can be derived from (6) where the corresponding filter factors are equal to zero or one. The terms up to and including λ_t are included in the summation and have a filter factor of one whilst the remaining terms are zero. The performance of TSVD regularization is often indistinguishable from that of a zero-order Tikhonov regularization [20].

A.3 Greensite Epicardial Formulation

Standard regularization techniques (such as Tikhonov and TSVD) have achieved only limited success in solving the inverse problem of electrocardiography [14]. The major drawback with these regularization schemes is that they impose non-physiological constraints on the problem by ignoring the temporal dependency of the data [24].

Attempts have been made to make better use of the temporal correlations by implementing explicit constraints based on solutions at adjacent time instances. Since cardiac activation is a continuous process in time it seems logical to incorporate the continuous property of the temporal information into the problem. This can be achieved via a Twomey technique [25]. However, this requires an initial estimate of the solution and the quality of the inverse solution depends on the quality of this estimate [13]. The major problem which such a technique is that the final solution will be biased towards the initial estimate of the solution.

Greensite describes the inappropriateness of such methods [24] and introduces a new method for computing epicardial potentials [17]. This method simultaneously regularizes the equations associated with each time point and is based on the idea (and proved theoretically) that a solution based on optimal regularization of each integral equation associated with each principle component of the data will be more accurate than a solution based on the optimal regularization of each integral equation associated with each time point.

Instead of treating each column of $\phi_B(\boldsymbol{x},t)$ independently, we can treat the body surface potentials as a *family* of solutions. The SVD of the body surface potential matrix $\boldsymbol{\Phi}_B \in \mathbb{R}^{M\times T}$ is given by

$$\phi_B(\boldsymbol{x},t) = \boldsymbol{U}_B\boldsymbol{\Sigma}_B\boldsymbol{V}_B^T = \sum_i u_{B,i}(\boldsymbol{x})\sigma_{B,i}v_{B,i}(t) \tag{12}$$

where $\boldsymbol{U}_B$ is an $M \times N_e$ matrix which represents the spatial basis, $\boldsymbol{\Sigma}$ is an $N_e \times N_e$ matrix with the singular values stored on the diagonal and $\boldsymbol{V}_B$ is a $S \times N_e$ matrix which represents the temporal basis where $N_e = \min(M,T)$ in reduced form. Thus (3) can be written as

$$\begin{aligned}\phi_H(\boldsymbol{y},t) &= \boldsymbol{A}^{\dagger}_{\lambda_t}[\phi_B(\boldsymbol{x},t)] \\ &= \sum_i \left[\sigma_{B,i}\boldsymbol{A}^{\dagger}_{\lambda_t}[u_{B,i}(\boldsymbol{x})]\right] v_{B,i}(t)\end{aligned} \tag{13}$$

The regularization parameter λ_t is the same for each i in (13) and thus the solution cannot possibly result in an optimum regularized solution [21]. This argument was justified as the term $\sigma_{B,i}u_{B,i}(\boldsymbol{x})$ represents almost pure noise for sufficiently large values of i. Instead of regularizing the solution with the same regularization parameter for each i a better approach is to remove the equations that represent the noise.

The solution method defined by Greensite [21] is

$$\phi_H(\boldsymbol{y},t) = \sum_i \sigma_{B,i}\boldsymbol{A}^{\dagger}_{\lambda_i}[u_{B,i}(\boldsymbol{x})]v_{B,i}(t) \tag{14}$$

where $\boldsymbol{A}^{\dagger}_{\lambda_i}$ is the regularised inverse of $\boldsymbol{A}$ for each individual equation i determined via either Tikhonov regularization with regularization parameter λ_i or TSVD regularization with a truncation rank λ_i.

We simplify the solution process of (14) by solving a two step problem, emphasizing that the solution process is best examined as a problem coupled with the regularized inverse regime.

We initially solve the system of linear equations for each equation i, *i.e.,*

$$u_{B,i}(\boldsymbol{x}) = \boldsymbol{A}[\gamma_i(\boldsymbol{y})] \tag{15}$$

The solution to (15) is obtained by

$$\gamma_i(\boldsymbol{y}) = \boldsymbol{A}^{\dagger}_{\lambda_i}[u_{B,i}(\boldsymbol{x})] \tag{16}$$

i.e., a traditional inverse method (*e.g.,* Tikhonov or TSVD) but applied to $u_{B,i}(\boldsymbol{x})$, the spatial basis vectors, rather than $\phi_B(\boldsymbol{x},t)$. Thus in the context of a zero-order Tikhonov regularization the solution to (16) is given by

$$\gamma_i(\boldsymbol{y}) = \sum_{n=1}^{N}\langle u_{A,n}(\boldsymbol{x}), u_{B,i}(\boldsymbol{x})\rangle \frac{\sigma_{A,n}}{\sigma_{A,n}^2 + \lambda_i^2} v_{A,n}(\boldsymbol{y}) \tag{17}$$

and similarly for TSVD

$$\gamma_i(\boldsymbol{y}) = \sum_{n=1}^{\lambda_i} \frac{\langle u_{A,n}(\boldsymbol{x}), u_{B,i}(\boldsymbol{x})\rangle}{\sigma_{A,n}} v_{A,n}(\boldsymbol{y}) \tag{18}$$

Finally the solution to (2) is given by

$$\phi_H(\boldsymbol{y}, t) = \sum_i \sigma_{B,i}\gamma_i(\boldsymbol{y})v_{B,i}(t) \tag{19}$$

or similarly in matrix form

$$\boldsymbol{\Phi}_H = \boldsymbol{\Gamma}\boldsymbol{\Sigma}_B\boldsymbol{V}_B^T \tag{20}$$

where $\gamma_i(\boldsymbol{y})$ forms the i-th column of the matrix Γ.

In a practical case the exact solution $\boldsymbol{\Phi}_H$ is unknown and it is necessary to have alternative technique to generate a solution as close to the optimal regularized solution as possible. The associated regularization parameter or truncation rank for each equation i can be determined via visual inspection of the discrete Picard condition [17]. To determine whether the discrete Picard condition in the manner presented in [17] is met is a subjective process. In our case, the determination of the inter-equation truncation rank was obtained in an automated manner. This was achieved via an estimate of the effective rank of the spatial signal data. This inter-equation rank was determined from the maximum curvature of the singular values of values of $\sigma_{B,i}$ and was used to determine an "optimal" regularized solution. However, in general, this solution will not be the global optimal solution obtained from choosing the optimal inter-equation rank.

B. Activation Based Inverse Algorithm

The activation inverse algorithm revolves around obtaining an estimate of the activation sequence from known body surface potentials. Using this estimate, the activation sequence is then refined using an optimization loop which minimizes the differences between the known torso potentials and those computed using the transfer matrix and the current estimate of the activation field.

The initial estimate is obtained by using the Critical Point Theorem (CPT) [19]. The CPT states that, a point $\boldsymbol{y}'$ on the the surface of the heart is a *critical point* of the activation time field $\tau\,(\boldsymbol{y})$ on the surface of the heart if and only if $A\,(\boldsymbol{y}', \boldsymbol{x})$ is in the space spanned by the spatial principal components of $\phi_B(\boldsymbol{x}, t)$. The activation field $\tau\,(\boldsymbol{y})$ is defined as the time at which phase zero of the action potential occurs at a point $\boldsymbol{y}$ on the surface of the heart.

The basic idea behind the CPT stems from the observation that when an evolving cardiac wave front intersects the endocardial or epicardial surface a *hole* develops in the wave front. This hole corresponds to a critical point and the time at which this occurs is known as the critical time. With all critical points and times determined, the computation of the entire activation field on both epicardial and endocardial surfaces is theoretically a well-posed problem [26].

In the noisy settings encountered in practice, the CPT does not always accurately locate the critical events. In general, the locations of the critical points are well determined but their corresponding times tend to be compressed towards the center of the time domain. As a result of this, the optimization phase of the procedure can be aided by the imposition of additional constraints on the optimization process. These constraints can include fixing the locations of critical points and the addition of a surface Laplacian constraint [27], [28] to ensure that the activation field is physiologically realistic. The surface Laplacian is a second order Tikhonov constraint, however, unlike the use of this constraint in epicardial potential approaches, it has a physiological basis since the path of the surface activation wavefront is known to be continuous and smooth at a length scale greater than the size of a cell. The surface Laplacian was computed using a finite difference approximation at the nodal positions.

The final objective function which is minimized with respect to the activation times is,

$$\tau\left(\boldsymbol{y}\right) = \min\left\{\|\boldsymbol{A}\phi_M(\boldsymbol{y},t) - \phi_B(\boldsymbol{x},t)\|_2^2 + \lambda\|\boldsymbol{L}\tau\left(\boldsymbol{y}\right)\|_2^2\right\} \tag{21}$$

where ϕ_M is the transmembrane potential, λ is a parameter controlling the degree of regularization imposed on the objective function and $\boldsymbol{L}$ is the surface Laplacian of the activation field.

The non-linear optimization process was described in detail in [19] along the computation of the approximation of the surface Laplacian. These methods were later extended to include an initial estimate given by the CPT in [29].

C. Determining the Regularization Parameters

All of the inverse algorithms mentioned above involve determining the appropriate level of regularization to include in the system. This involves determining at least one regularization parameter for which there exist many *a posteriori* methods to determine this value. Each method attempts to provide a balance between the solution and regularization norm. Commonly accepted methods are generalized cross validation [30], L-curve [31], zero-crossing [32] or the CRESO criterion [33].

We use the formulation for the standard potential inverse given in (1) for determining the appropriate regularization parameters. The same methods apply for Greensite's approach except $u_{B,i}(\boldsymbol{x})$ replaces $\phi_B(\boldsymbol{x},t)$ and $\gamma_i(\boldsymbol{y})$ replaces $\phi_H\left(\boldsymbol{y},t\right)$ in (15).

Since the matrices $\boldsymbol{U}_A$ and $\boldsymbol{V}_A$ are orthonormal the squared solution norm of (6) is given as

$$\|\phi_H\left(\boldsymbol{y},t\right)\|_2^2 = \sum_{n=1}^{N}\left[f_n(t)\frac{\langle u_{A,n}(\boldsymbol{x}),\,\phi_B(\boldsymbol{x},t)\rangle}{\sigma_{A,n}}\right]^2 \tag{22}$$

and the residual term is given as

$$\|\boldsymbol{A}\phi_H\left(\boldsymbol{y},t\right) - \phi_B(\boldsymbol{x},t)\|_2^2 = \sum_{n=1}^{N}\Big[\big((1-f_n(t)\big)\langle u_{A,n}(\boldsymbol{x}),\phi_B(\boldsymbol{x},t)\rangle\Big]^2 \tag{23}$$

We define and use four criteria for obtaining an appropriate regularization parameter or truncation rank.

C.1 Optimal Criterion

The optimal criterion solution, although clinically not feasible as it requires *a priori* knowledge of the epicardial potential distribution, places a lower bound for the accuracy of a given regularization scheme and thus leads to a valid comparison measure between relative regularization inverse approaches.

The optimal solution for Tikhonov and TSVD regularization schemes can be obtained by choosing the optimal regularization parameter λ_t at time t for the solution to (3) which minimizes (24)

$$\|\hat{\boldsymbol{\phi}}_{H,i}(\boldsymbol{y}) - \boldsymbol{\phi}_{H,i}(\boldsymbol{y})\|_2 \tag{24}$$

where $\hat{\boldsymbol{\phi}}_{H,i}$ are the i-th regularized solution and forms the i-th column of the regularized solution $\boldsymbol{\Phi}_H$. The optimal regularized solution to Greensite's method can be obtained via regularizing every i-th equation individually since the columns of $\boldsymbol{U}_B$ are orthogonal, hence are linearly independent. Thus for every solution $\gamma_i(\boldsymbol{y})$ to (16) the optimal regularization parameter is the value which minimizes

$$\|\boldsymbol{\Gamma}\boldsymbol{\Sigma}_B\boldsymbol{V}_B^T - \boldsymbol{\Phi}_H\|_F \tag{25}$$

where $\|\cdot\|_F$ denotes the *Frobenius* norm.

C.2 L-Curve

The L-curve approach involves plotting a log-log plot of the residual norm on the abscissa against the solution norm on the ordinate. The resulting curve is typically in the form of an "L" with the regularization parameter λ_t defined as a point on the L-curve defined by

$$(\zeta(\lambda_t), \eta(\lambda_t)) = (\log\|\boldsymbol{A}\phi_H(\boldsymbol{y}, t) - \phi_B(\boldsymbol{x}, t)\|_2, \log(\phi_H(\boldsymbol{y}, t)\|_2) \tag{26}$$

The L-curve criterion determines the resulting regularization parameter as the corner of the "L" which is associated with the maximum curvature $\boldsymbol{\kappa}$, defined for an implicit function as

$$\kappa(\lambda_t) = \frac{\zeta'\eta'' - \zeta''\eta'}{((\zeta')^2 + (\eta')^2)^{3/2}} \tag{27}$$

C.3 CRESO

The Composite REsidual and Smoothing Operator (CRESO) criterion chooses the regularization parameter for which the difference between the derivative of the residual term and the derivative of the smoothing term is maximized [33].

The CRESO regularization parameter is determined as the smallest value of λ_t that results in a relative maximum of the function

$$C(\lambda_t) = \|\phi_H(\boldsymbol{y}, \lambda_t)\|_2^2 + 2{\lambda_t}^2 \frac{d}{d\lambda_t} \|\phi_H(\boldsymbol{y}, \lambda_t)\|_2^2 \tag{28}$$

where $\phi_H(\boldsymbol{y}, \lambda_t)$ is the potentials on the heart regularized by the regularization parameter λ_t.

The function $C(\lambda_t)$ is the derivative of the function $B(\lambda_t)$, where

$$B(\lambda_t) = \lambda_t^2 \|\phi_H(\boldsymbol{y}, \lambda_t)\|_2^2 - \|\boldsymbol{A}\phi_H(\boldsymbol{y}, \lambda_t) - \phi_B(\boldsymbol{x}, t)\|_2^2 \tag{29}$$

The CRESO function is only strictly defined for a continuous regularization parameter and hence cannot be used for the discrete TSVD approximation [34].

C.4 Zero-Crossing

The zero-crossing criterion aims to find the regularization parameter via solving the function $B(\lambda_t) = 0$ in (29) for the smallest value of λ_t. This is essentially the minimum-product criterion proposed by [34] as another approach of obtaining the corner from the L-curve [35].

III. Geometric and Cardiac Source Models

To test and compare the various inverse approaches a geometrical model and cardiac source configurations is required. For the inverse algorithms to be widely accepted as an aid for clinical diagnosis some form of validation of results is essential. We aim to validate these results using invasively measured data obtained from pigs [36] and for this reason, our simulations studies have concentrated on using porcine geometry and have included cardiac sources obtained from pig experiments.

A. Geometric Model

The boundary element based porcine model was developed from a sequence of 5 mm spaced cross-sectional CT images of a young 20 kg pig. Three-dimensional data sets of the key surfaces of the organs were digitized (left and right endocardial, epicardial, lung and skin) and bicubic Hermite elements were then used to model each surface using a non-linear fitting technique [37]. The appropriate mesh resolution for the torso model was determined by performing a detailed convergence analysis. Additional details of the model construction and convergence process can be found in [29].

B. Cardiac Source Models

In order to solve the forward problem of electrocardiography a cardiac source is required which defines the electrical distribution, usually as an activation sequence or potential distribution. The source can consist of actual heart potential recordings, obtained via invasive means, can be approximated using simulated models or can be approximated from recorded sources which are thought to represent a realistic epicardial potential distribution.

The inverse problem is inherently non-linear, so three different cardiac sources were used throughout this study. They included an activation field derived from specified initial activation sites (*double point*), an activation field derived from and eikonal simulation (*eikonal*) [38] of ventricular activation and an activation field obtained from an experimental setup (*experimental*) [36].

The double point cardiac source (shown in Fig. 1a) was generated from two initial activation sites located near the left and right free epicardial walls. The activation time for both the endocardium and epicardium surfaces were based on a distance measure from the nearest activation site . The left activation point source was further from the epicardium which represents a delayed pulse. Despite being a simplistic theoretical activation sequence, it has the basic features of a real activation sequence and is a useful test case on which to compare the various inverse procedures.

[Figure 1 about here.]

The eikonal cardiac source (shown in Fig. 1b) was derived from a simulation of a myocardial wavefront modeled using an eikonal equation [38]. Although a numerical solution, it possesses the correct activation properties of a normal activation sequence [39]. The original solution was performed on a canine ventricle model and this was then transformed to the porcine ventricular surfaces via an orthogonal projection and least squares fitting of the activation field.

The experimental cardiac source (shown in Fig. 1c) was derived from epicardial surface potentials which were experimentally recorded *in-vivo* from a porcine specimen [36]. The epicardial potentials were measured using an electrode sock with 127 electrodes. The activation times were defined as the point at which the signal tracings had the greatest negative slope as determined via a moving finite difference interval. The measured epicardial potential field was then fitted in a least-squares sense to the heart mesh. A realistic endocardial activation sequence was then generated in accordance with the epicardial sequence from a myocardial activation inverse simulation using clean, forwardly mapped body surface potential from the recorded epicardial distribution to preserve consistency.

The relative short duration of the experimental cardiac source is because it was obtained from a normal sinus rhythm from a porcine heart. Its duration is of the correct length when compared to a normal porcine QRS duration [36].

IV. Inverse Solutions

By analyzing inverse solutions obtained from a simulation study, the results will not be affected in an unknown manner by any experimental errors (which always occur in an experimental or clinical setup). The performances of different algorithms can also be systematically compared when they are subjected to known levels of different experimental errors (*e.g.*, signal, geometric or material property errors).

A. The Forward and Inverse Problems

The appropriate transfer matrices to compute both the body surface potentials and epicardial potentials for the porcine model were assembled using the methods and material conductivities described in [29]. For each of the three cardiac sources described in Sec. III, corresponding epicardial and torso surface potentials were computed using the appropriate transfer matrices. These are capable of providing known potential and activation time solutions on all locations throughout the torso. These torso surface potentials where then used as input for the each of inverse algorithms. The resultant inverse solutions were then compared to the known activation and epicardial potential solutions.

B. Solution Comparison

When performing a numerical simulation study it is possible to directly compare the numerical inverse solutions to the known or goal solutions. This direct comparison provides an accurate quantitative measure of the performance of each inverse algorithm. Using these methods the relative performances of each algorithm can also be systematically compared under different conditions.

Known solution fields $\boldsymbol{\tau}$ were thus compared to the computed $\hat{\boldsymbol{\tau}}$ solutions using the error metrics described in (30), (31) and (32).

The differences between the two activation fields can be quantified in terms of the RMS error given by

$$\text{RMS error} = \left[\frac{(\tau_n - \hat{\tau}_n)^2}{N}\right]^{\frac{1}{2}} \tag{30}$$

where τ_n represents the correct activation field and $\hat{\tau_n}$ is the computed activation field and N is the number of sample locations.

The relative RMS error provides a normalized error measure for differences in magnitudes of two fields and is defined as

$$\text{Relative RMS} = \left[\frac{\tau_n - \hat{\tau_n}^2}{\tau_n^2}\right]^{\frac{1}{2}} \tag{31}$$

When used to compare signal traces, this error metric can provide a relative difference in the magnitude of the signals.

The Similarity Index (SI) or correlation coefficient, measures the linear relationship between the two fields and is insensitive to magnitude differences. It is defined as

$$\mathrm{SI} = \frac{\tau_n - \bar{\tau}_n}{\|\tau_n - \bar{\tau}_n\|_2} \cdot \frac{\hat{\tau}_n - \bar{\hat{\tau}}_n}{\|\hat{\tau}_n - \bar{\hat{\tau}}_n\|_2} \tag{32}$$

where $\bar{\tau_n}$ denotes the sample mean. A SI coefficient of 1.0 indicates the two fields have an identical pattern.

The epicardial potential and myocardial activation based inverse formulations produce distinctly different solutions, one of the solutions must be converted to a compatible format so that they can be compared. When mapping arrhythmias, activation times provide useful information regarding the points of initial activation and the path of electrical excitation, therefore, the epicardial solutions were converted to activation time solutions by assigning the point of maximum negative slope as the activation time [40]. This conversion process introduces further errors into the potential based solutions and one might argue that this biases the activation based methods. However, it is fair to compare how well the epicardial potentials estimate activation times, versus how well the activation based formulations estimate activation times since the time of activation is of high importance in a clinical situation, especially when examining arrhythmias. The degree of error introduced in an epicardial potential estimate of activation time is illustrated in three cases shown in Fig. 2 where the activation times derived from maximum negative slope are compared to the original activation from which the epicardial potentials were computed. Minimal, average and maximal errors are shown for a given data set with errors of 0.2, 1.0 and 9.4 ms respectively.

[Figure 2 about here.]

Another source of error associated with epicardial inverse activation time is that the activation times obtained are discrete time measures and hence an error of up to 0.5 ms can be associated at each heart node.

C. Inverse Simulations with Electrical Noise

The porcine model with all six regions was used to compare each of the inverse algorithms under moderate noise conditions. Torso surface potentials were generated by solving the forward problem for each of the cardiac sources. Gaussian noise of 50 μV RMS were applied to the body surface signals (peak-to-peak range of around 3 mV) and then used as input for each of the inverse algorithms. This a realistic low level of Gaussian noise which represents a typical error obtained in an experimental or clinical situation.

The results for these simulations are summarized in Fig. 3 and are shown graphically for the activation and Greensite-Tikhonov method using the zero-crossing criterion for determining the regularization parameter in Fig. 4 (*i.e.*, methods 1 and 11 respectively). Solutions computed with minimal level of 5 μV RMS of Gaussian noise with the double point cardiac source are shown as the ‘control’ simulations in Fig. 5 and Fig. 6.

[Figure 3 about here.]

[Figure 4 about here.]

The computed solutions were compared to the known cardiac sources with both the RMS and SI error metrics, with both producing similar trends in the results as shown in Fig. 3.

In the presence of 50 μV RMS noise the activation based approach performed the best for the double point and the experimental cardiac source, while the Tikhonov method with the regularization parameter determined using the CRESO criterion had the best results with the eikonal cardiac source. As shown by the control simulations from Fig. 5 and Fig. 6 where only 5 μV RMS noise is present, the potential based methods produced the best solutions when the optimal regularization parameter was used. In general, no inverse approach was clearly the best, however, the Greensite-Tikhonov method with the regularization methods determined using the zero-crossing and L-curve methods may be slightly favored under moderate levels of Gaussian noise.

D. Inverse Simulations with Heart Displacement

The inverse simulations were then performed with the inclusion of a correlated geometric error. This correlated error involved displacing the heart by a known amount in the lateral directions from its original position. This error provides an example of a typical error that can be experienced in an experimental situation when the model of the heart is not correctly positioned. The translation of the heart produces a correlated error on the system and most inverse algorithms are geared towards filtering out the effects of uncorrelated errors such as Gaussian signal noise. To represent true conditions a minimal level of 5 μV RMS of Gaussian noise was added in each simulation.

[Figure 5 about here.]

[Figure 6 about here.]

Fig. 5 and Fig. 6 illustrates the effects of introducing varying levels of geometric error into the system. Fig. 5 compares the solutions of all the inverse methods (after the potential based solutions have been converted to activation fields) while Fig. 6 compares each of the potential based solutions against the known epicardial potential distributions.

Fig. 5 shows that the activation based method produced results which were more stable than the potential based methods in the presence of geometrical error. However, when no geometric error was added and combined with only 10 μV RMS of Gaussian noise the potential based methods consistently produced slightly better results. However, this was not the case when 50 μV RMS of Gaussian noise was added to the torso surface signals as the results show in Fig. 3a, where the potential based methods tended to out perform the activation based method. Large errors usually resulted in the potential based solutions when the heart was displaced by greater than 10 mm from its original position.

When choosing the optimal regularization parameter for each potential based method, all inverse schemes produced similar results, under all levels of geometric error. However, these methods are not usually practical as they require *a priori* knowledge of the heart solution.

The Greensite-Tikhonov methods with the regularization parameter determined using the L-curve and zero-crossing methods produced the best results in the presence of geometric noise for each of the potential based methods. This was the case when the solutions were compared to the original epicardial potential solutions or converted and then compared to the original activation times.

In Fig. 7 we also compare the performance of the Tikhonov which only regularizes the the spatial domain and the Greensite-Tikhonov inverse method which regularizes in both the spatial and temporal domain. In both methods the zero-crossing method is used to determine the level of regularization to include. The plots show traces from two locations on the epicardium with the heart displaced either 10 or 20 mm. The solutions produced by the Greensite-Tikhonov method does not contain high frequency oscillations which are undesirable especially when activation times are derived by picking the point of maximum negative slope.

[Figure 7 about here.]

In the absence of correlated errors and low levels of electrical noise, the potential based methods tended to perform slightly better than the activation based approach. The Greensite-Tikhonov method using CRESO to determine the regularization parameter produced the best results under control conditions. However, all potential based methods failed drastically as soon as any geometric error was introduced into the system, while the activation based methods did not.

V. Discussion

The lack of controlled simulation studies comparing the effectiveness of the vast variety of inverse algorithms has lead to uncertainty regarding the relative performances of each of the algorithms. The different protocols applied to each of the previous simulation studies also means there are difficulties in comparing the results between different studies.

We have presented the initial results from a simulation study using a realistic porcine model. The results from this study are intended to aid in the understanding of the levels of accuracy required for the inputs of the inverse problem to obtain viable solutions as well as to determine the relative performance of different inverse procedures.

The simulations have involved three distinctly different cardiac sources and a variety of inverse algorithms. In addition to control conditions, the algorithms have been also been subjected to the presence of signal, material property and geometric errors, although only the results examining the effect of lateral heart translation have been presented at this stage.

As Fig. 3 shows, the accuracy of the solution is highly dependent on the complexity of the cardiac source. However, it is reassuring that all inverse methods tended to perform at a similar level for each cardiac source indicating that it is not necessary to use different algorithms to reconstruct different cardiac sources.

The errors introduced when epicardial potentials are converted to activation based solutions, though significant at times, does provide a common basis for the different solutions to be compared. By examining Fig. 5 and Fig. 6 similar trends are maintained after the conversion process, so the converted results still provide a true representation of the potential based solution.

The activation based inverse method produced the most accurate inverse solutions in the presence of geometrical error. However, when no geometric error was present in the system (something not achievable in practice), the potential based approaches were marginally favored. When the heart was laterally translated more than 10 mm in either direction, the accuracy of the epicardial potential based solutions began to deteriorate rapidly. Using the optimal criterion each of the potential based methods provided similar results, but this method of selecting the regularization parameter is not usually feasible as it requires *a priori* knowledge of the solution. The Greensite-Tikhonov solutions with the regularization parameter determined using the CRESO and zero-crossing methods produced the most favorable potential based solutions.

The consistency of the activation based approach indicates that is may be favored in a clinical situation. This approach is also able to provide information about the electrical activity on both the epicardial and endocardial surfaces of the heart (often the location where catheter based recordings are obtained) while the potential based methods only provide information on the epicardial surface. The potential based approaches are however, less computationally expensive and can provide solutions on a near real-time basis. Thus a combined potential-activation based inverse method may be the preferred approach to a clinically viable inverse procedure.

ACKNOWLEDGMENTS

All authors would like to acknowledge Drs. Martyn Nash, Chris Bradley and David Paterson of the The Cardiac Autonomic Control Research Group at the Oxford University for supplying the CT data for the geometric model and the experimental data required for the experimental cardiac source and Dr. Karl Tomlinson for supplying the data for the eikonal cardiac source model. The first author would like to acknowledge financial assistance provided through an Auckland UniServices Ltd. Scholarship.

REFERENCES

[1] D. H. Brooks and R. S. MacLeod, “Electrical imaging of the heart,” *IEEE Signal Processing Magazine*, vol. 14, pp. 24–42, Jan. 1997.

[2] Y. Rudy and B. J. Messinger-Rapport, "The inverse problem in electrocardiography: Solutions in terms of potentials," *Crit. Rev. Biomed. Eng.*, vol. 16, no. 3, pp. 215–268, 1988.

[3] Y. Yamashita, "Theoretical studies on the inverse problem in electrocardiography and the uniqueness of the solution," *IEEE Trans. Biomed. Eng.*, vol. 29, pp. 719–725, Nov. 1982.

[4] R. C. Barr, M. S. Spach, and G. S. Herman-Giddens, "Selection of the number and positions of measuring locations for electrocardiography," *IEEE Trans. Biomed. Eng.*, vol. 18, pp. 125–138, Mar. 1971.

[5] R. L. Lux, C. R. Smith, R. F. Wyatt, and J. A. Abildskov, "Limited lead selection for estimation of body surface potential maps in electrocardiography," *IEEE Trans. Biomed. Eng.*, vol. 25, pp. 270–276, May 1978.

[6] L. Zablow, "An equivalent cardiac generator which preserves topography," *Biophys. J.*, vol. 6, p. 535, 1966.

[7] R. O. Martin and T. C. Pilkington, "Unconstrained inverse electrocardiography: Epicardial potentials," *IEEE Trans. Biomed. Eng.*, vol. 19, pp. 276–285, July 1972.

[8] R. C. Barr and M. S. Spach, "Inverse calculation of QRS-T epicardial potentials from body surface potential distributions for normal and ectopic beats in the intact dog," *Circ. Res.*, vol. 42, pp. 661–675, 1978.

[9] M. S. Spach and R. C. Barr, "Ventricular intramural and epicardial potential distributions during ventricular activation and repolarization in the intact dog," *Circ. Res.*, vol. 37, pp. 243–257, 1975.

[10] J. Cuppen and A. van Oosterom, "Model studies with the inversely calculated isochrones of ventricular depolarization," *IEEE Trans. Biomed. Eng.*, vol. 31, pp. 652–659, 1984.

[11] J. Hadamard, *Lectures on Cauchy's Problems in Linear Partial Differential Equations*. New Haven: Yale University Press, 1923.

[12] A. Tikhonov and V. Arsenin, *Solution of ill-posed problems*. Washington, D.C.: John Wiley & Sons, 1977.

[13] H. Oster and Y. Rudy, "The use of temporal information in the regularization of the inverse problem of electrocardiography," *IEEE Trans. Biomed. Eng.*, vol. 39, pp. 65–75, 1992.

[14] D. H. Brooks, G. F. Ahmad, R. S. MacLeod, and G. M. Maratos, "Inverse electrocardiography by simultaneous imposition of multiple constraints," *IEEE Trans. Biomed. Eng.*, vol. 46, pp. 3–18, Jan. 1999.

[15] B. J. Messinger-Rapport and Y. Rudy, "The inverse problem in electrocardiography: A model study of the effects of geometry and conductivity parameters on the reconstruction of epicardial potentials," *IEEE Trans. Biomed. Eng.*, vol. 33, pp. 667–676, July 1986.

[16] P. R. Johnston and D. Kilpatrick, "The inverse problem of electrocardiology: The performance of inversion techniques as a function of patient anatomy," *Math. Biosci.*, vol. 126, pp. 125–146, Apr. 1995.

[17] F. Greensite and G. Huiskamp, "An improved method for estimating epicardial potentials from the body surface," *IEEE Trans. Biomed. Eng.*, vol. 45, pp. 98–104, Jan. 1998.

[18] F. Greensite, "Remote reconstruction of confined wavefront propagation," *Inverse Problems*, vol. 11, pp. 361–370, 1995.

[19] G. Huiskamp and F. Greensite, "A new method for myocardial activation imaging," *IEEE Trans. Biomed. Eng.*, vol. 44, pp. 433–446, June 1997.

[20] P. C. Hansen, "Analysis of discrete ill-posed problems by means of the L-curve," *SIAM Review*, vol. 34, pp. 560–580, Dec. 1992.

[21] F. Greensite, "Second-order approximation of the pseudoinverse for operator deconvolutions and families of ill-posed problems," *SIAM J. Appl. Math.*, vol. 59, no. 1, pp. 1–16, 1998.

[22] B. J. Messinger-Rapport and Y. Rudy, "Regularization of the inverse problem of electrocardiology: A model study," *Math. Biosci.*, vol. 89, pp. 79–118, 1988.

[23] P. C. Hansen, *Rank-Defficient and Discrete Ill-Posed Problems: Numerical Aspects of Linear Inversion.* Philadelphia: Society for Industrial and Applied Mathematics, 1998.

[24] F. Greensite, *Computational Inverse Problems in Electrocardiography*, ch. 5: Myocardial Activation Imaging, pp. 143–190. Advances in Computational Biomedicine, Southampton, UK: WIT Press, 2001.

[25] S. Twomey, "On the numerical solution of Fredholm integral equations of the first kind by the inversion of the linear system produced by quadrature," *J. Assoc. Comput. Mach.*, vol. 10, pp. 97–101, 1963.

[26] F. Greensite, "Some imaging parameters of the oblique dipole layer cardiac generator derivable from body surface electrical potentials," *IEEE Trans. Biomed. Eng.*, vol. 39, pp. 159–164, Feb. 1992.

[27] G. J. Huiskamp and A. van Oosterom, "The depolarization sequence of the human heart surface computed from measured body surface potentials," *IEEE Trans. Biomed. Eng.*, vol. 35, pp. 1047–1059, Dec. 1988.

[28] T. F. Oostendorp and A. van Oosterom, "Interpolation on a triangulated 3D surface," *J. Comput. Phys.*, vol. 80, pp. 331–343, 2 1989.

[29] A. J. Pullan, L. K. Cheng, M. P. Nash, C. P. Bradley, and D. J. Paterson, "Noninvasive electrical imaging of the heart: Theory and model development," *Ann. Biomed. Eng.*, vol. 29, pp. 817–836, Oct. 2001.

[30] G. H. Golub, M. T. Heath, and G. Wahba, "Generalized cross-validation as a method for choosing a good ridge parameter," *Technometrics*, vol. 21, pp. 215–223, 1979.

[31] P. C. Hansen and D. P. O'Leary, "The use of the L-curve in the regularization of discrete ill-posed problems," *SIAM J. Sci. Comput.*, vol. 14, pp. 1487–1503, Nov. 1993.

[32] P. R. Johnston and R. M. Gulrajani, "A new method for regularization parameter determination in the inverse problem of electrocardiography," *IEEE Trans. Biomed. Eng.*, vol. 44, pp. 19–39, Jan. 1997.

[33] P. Colli Franzone, L. Guerri, B. Taccardi, and C. Viganotti, "Finite element approximation of regularised solutions of the inverse potential problem of electrocardiography and applications to experimental data," *Calcolo*, vol. 22, no. 1, pp. 91–186, 1985.

[34] J. Lian, D. Yao, and B. He, "A new method for implementation of regularization in cortical potential imaging," in *Proceedings of the 20th Annual International Conference of the IEEE Engineering in Medicine and Biology Society*, vol. 20, (Hong Kong, China), pp. 2155–2158, IEEE Computer Society Press, 1998.

[35] P. R. Johnston and R. M. Gulrajani, "Selecting the corner of the L-curve approach to Tikhonov regularisation," *IEEE Trans. Biomed. Eng.*, vol. 47, pp. 1293–1296, Sept. 2000.

[36] M. P. Nash, C. P. Bradley, L. K. Cheng, A. J. Pullan, and D. J. Paterson, "An experimental-computational framework for validating *in-vivo* ECG inverse methods," *Intl. J. Bioelectromagnetism*, vol. 2, Sept. 2000.

[37] C. P. Bradley, A. J. Pullan, and P. J. Hunter, "Geometric modeling of the human torso using cubic Hermite elements," *Ann. Biomed. Eng.*, vol. 25, pp. 96–111, 1997.

[38] K. A. Tomlinson, A. J. Pullan, and P. J. Hunter, "Modeling myocardial excitation wavefront propagation in ventricles by finite element solution of an eikonal equation," in *Proceedings of the First Joint Meeting of BMES & IEEE/EMBS Conference*, (Atlanta, GA), p. 192, Oct. 1999.

[39] D. Durrer, R. T. van Dam, G. E. Freud, M. J. Janse, F. L. Meijler, and R. C. Arzbaecher, "Total excitation of the isolated human heart," *Circulation*, vol. 21, pp. 899–912, 1970.

[40] H. Oster, B. Taccardi, R. Lux, P. Ershler, and Y. Rudy, "Electrocardiographic imaging. Noninvasive characterization of intramural myocardial activation from inverse-reconstructed epicardial potentials and electrograms," *Circulation*, vol. 97, pp. 1496–1507, 1998.

LIST OF FIGURES

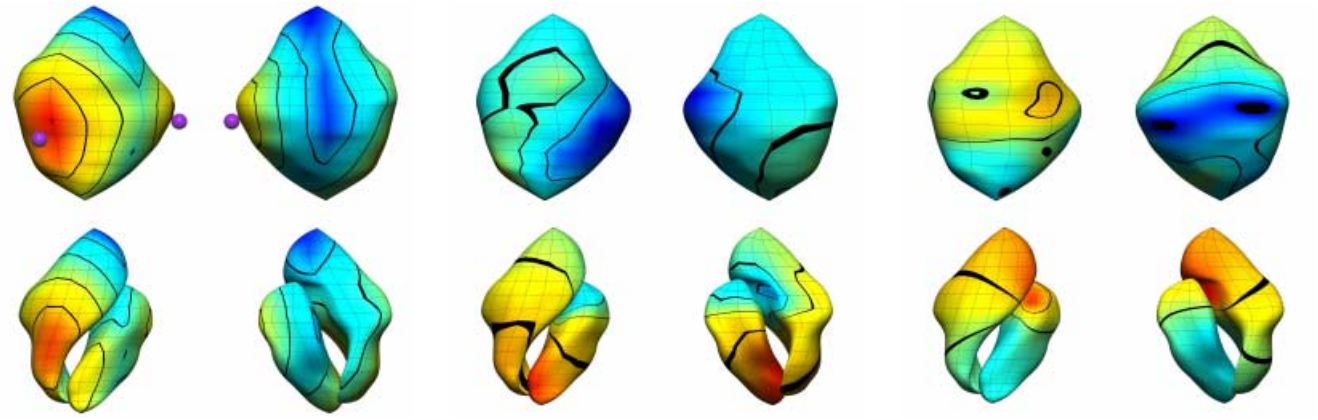

(a) Double Point (b) Eikonal (c) Experimental

Fig. 1. The three cardiac source models (double point, eikonal and experimental) shown with the color field representing the activation activation times (ms), red representing earliest activation and blue latest point of activation. Multiple views are shown of each cardiac source, with the epicardial surfaces shown in the top row and the endocardial surface on the bottom. Anterior views are shown in the first, third and fifth columns and posterior views in the second, fourth and sixth columns.

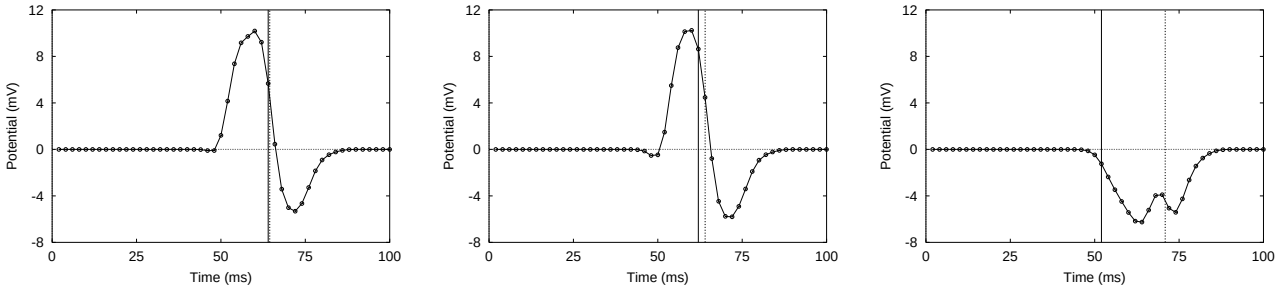

(a) (b) (c)

Fig. 2. Errors associated with the conversion of epicardial potentials to activation times. Activation times derived derived from maximum negative slope are compared to the original activation from which the epicardial potentials were computed. Minimal, average and maximal errors are shown for one data set with errors of 0.2, 1.0 and 9.4 ms respectively.

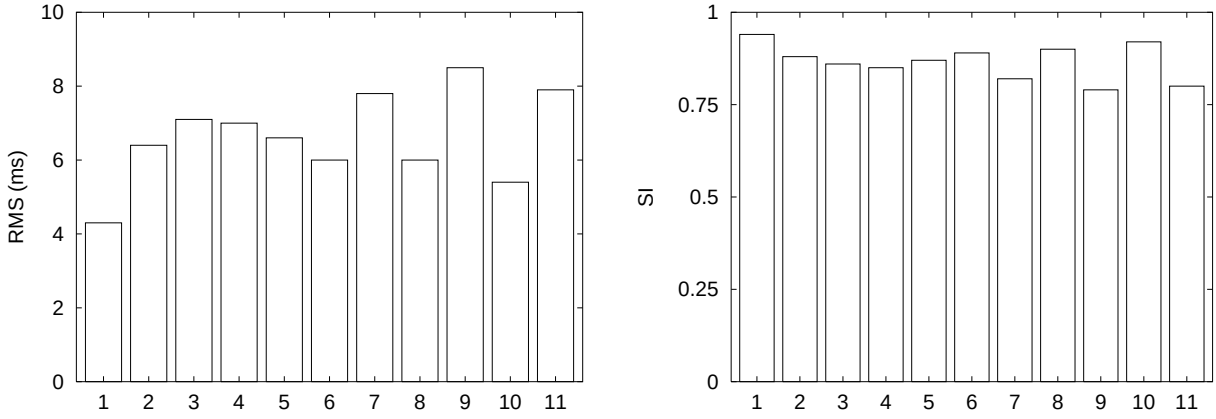

(a) Double Point Source

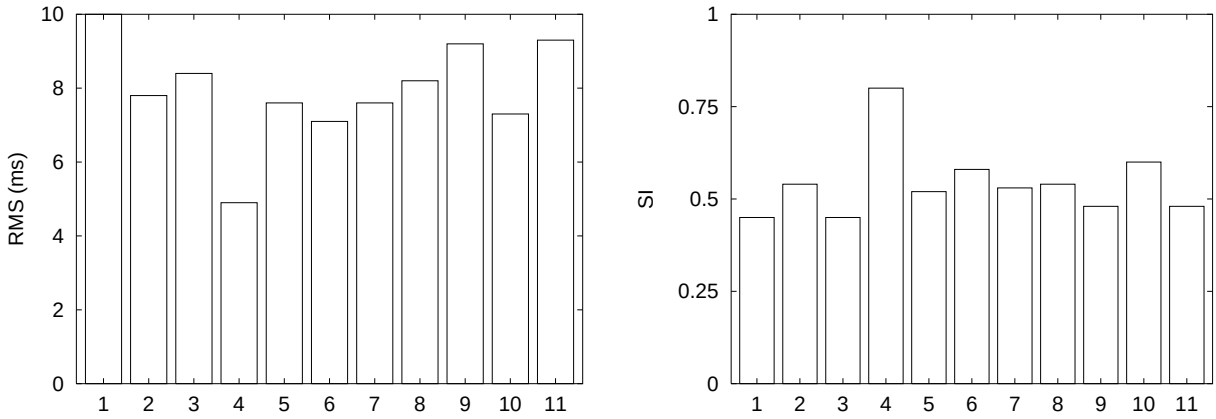

(b) Eikonal Source

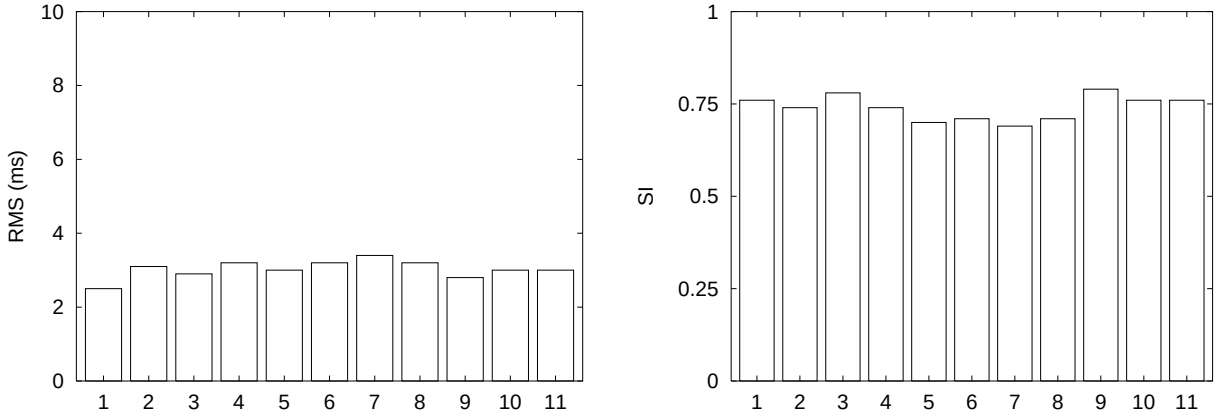

(c) Experimental Source

Fig. 3. Control simulations (with $50\ \mu$V RMS noise) performed with each of the three cardiac sources. Each bar indicates the results for a different inverse algorithm. (1) Activation with no regularization, (2) TSVD optimal regularization, (3) TSVD-Greensite optimal regularization, (4-7) Tikhonov CRESO/Lcurve/optimal/zero-crossing regularization and (8-11) Greensite-Tikhonov CRESO/Lcurve/optimal/zero-crossing regularization. The left column shows the solutions compared using RMS error and the right column compared using the SI index.

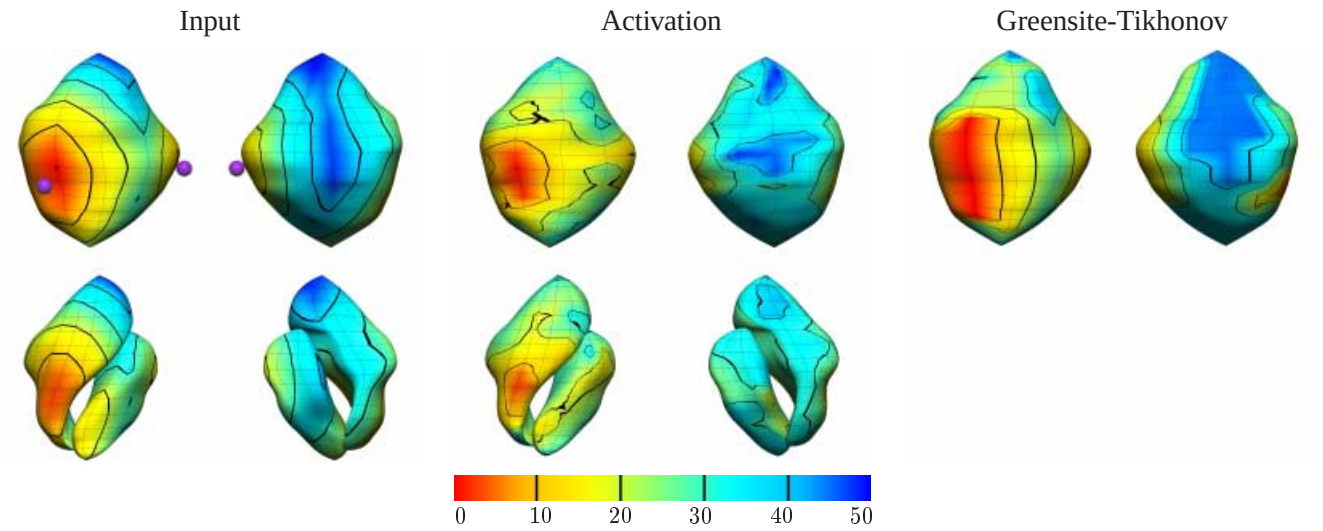

Fig. 4. Activation maps (ms) comparing the input double point source and the inverse computed solutions for the activation (1) and Greensite-Tikhonov approach and using the zero-crossing method (11) for determining the regularization parameter when subjected to 50 μV RMS of noise. The epicardial surfaces are shown in the top row and the endocardial surface on the bottom row. Shown are the input activation field (left two columns) and the inverted activation field (middle two columns) and the activation field from the Greensite-Tikhonov potential solution (right two columns). The colored field represents the activation times in ms, with red being earliest activation and blue latest activation. Anterior views are shown in the first, third and fifth columns and posterior views in the second and fourth and sixth columns. The purple spheres in the input source show the locations of the activation seed points used for generating the activation field.

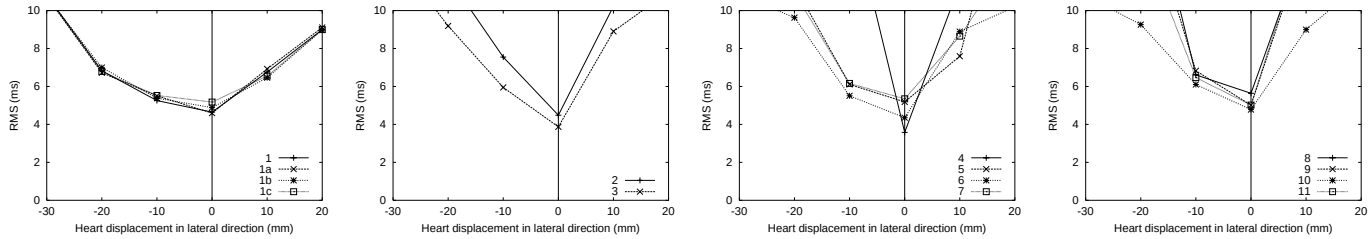

Fig. 5. Effect of heart displacement (with 10 μV RMS noise) when comparing activation based solutions using the double point source. The epicardial potential solutions have been converted to activation times so the solutions can be compared. The solutions for each technique have been compared to the exact solution using the RMS error and are plotted against the amount the heart has been displaced from is original position. The traces are labelled as follows: (1) Activation with no regularization, (1a-c) low/medium/high levels of regularization, (2) TSVD optimal regularization, (3) TSVD-Greensite optimal regularization, (4-7) Tikhonov CRESO/Lcurve/optimal/zero-crossing regularization and (8-11) Greensite-Tikhonov CRESO/Lcurve/optimal/zero-crossing regularization.

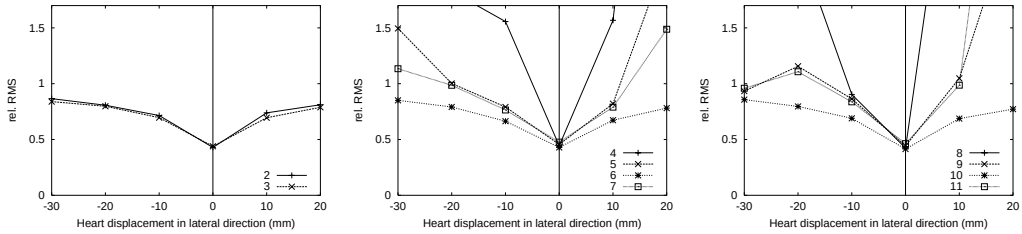

Fig. 6. Effect of the lateral heart displacement (with $10\ \mu$V RMS noise) on the various potential based algorithms using the double point source. The potential based results were directly compared to the known epicardial potentials solutions using the relative RMS error metric. Legends are as described in Fig. 5.

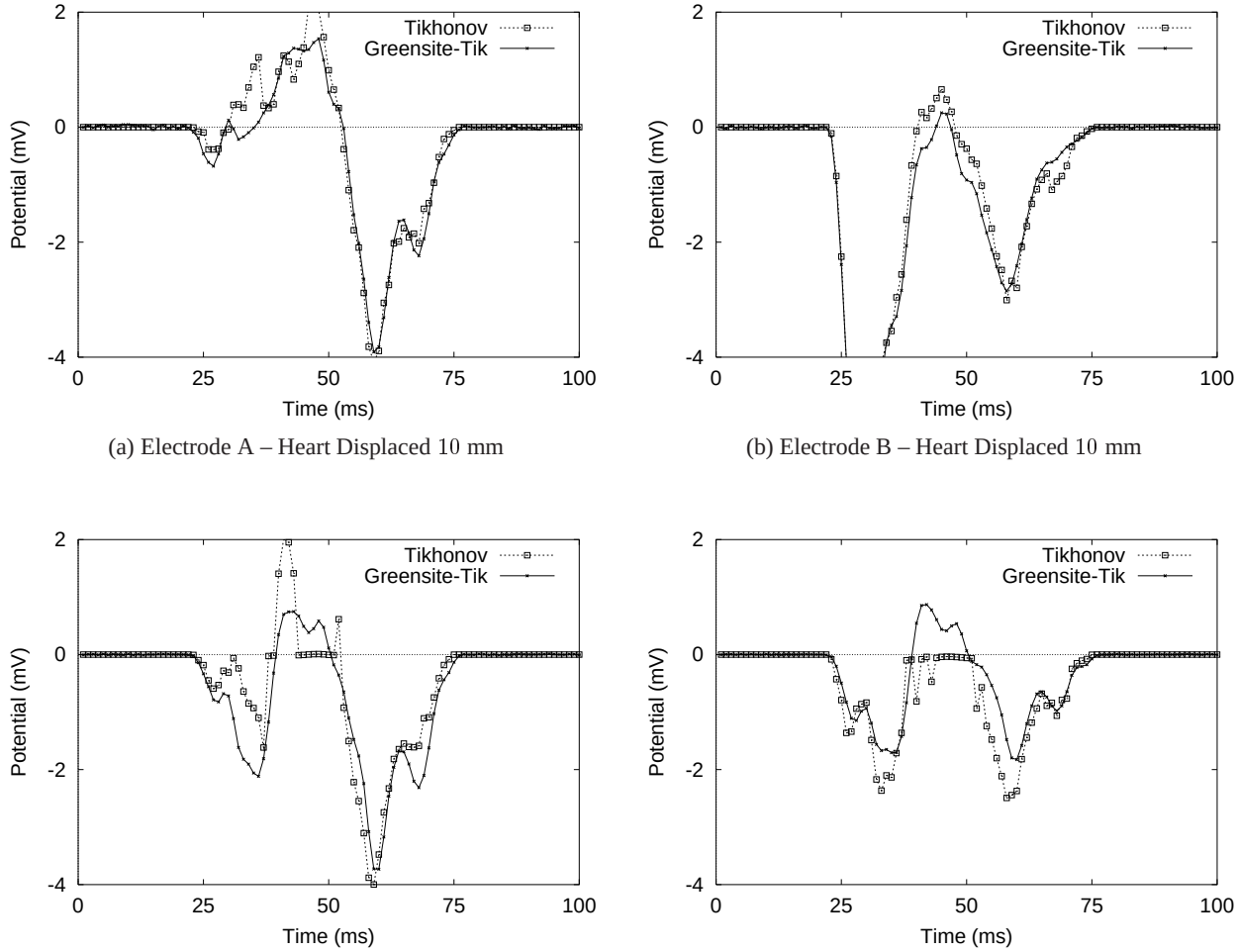

(a) Electrode A – Heart Displaced 10 mm

(b) Electrode B – Heart Displaced 10 mm

(c) Electrode A – Heart Displaced 20 mm

(d) Electrode B – Heart Displaced 20 mm

Fig. 7. Comparison of Tikhonov and Greensite-Tikhonov potential inverse methods under different levels of geometric error. Each plot compares the solutions obtained from the two potential based inverse methods using the zero-crossing method to determine the regularisation parameter. Shown in (a) and (b) are solutions where the heart has been laterally translated by 10 mm, while (c) and (d) compares solutions where the heart has been displaced by 20 mm. The tracings are shown for two different locations on the epicardium: Electrode A shown in (a) and (c) and Electrode B shown in (b) and (d). Each tracing shows that the Greensite-Tikhonov method produces solutions with less high frequency oscillations, especially when higher levels of geometric error are present in the system.